RESEARCH ARTICLE | DECEMBER 16 2024

Data-driven identification of the critical transition to thermoacoustic instability in a full-scale solid rocket motor

Guanyu Xu (徐冠宇) ; Bing Wang (王兵) ; Peijin Liu (刘佩进) ; Yu Guan (关昱)

Physics of Fluids 36, 124127 (2024)
https://doi.org/10.1063/5.0246774

Physics of Fluids ARTICLE pubs.aip.org/aip/pof

Data-driven identification of the critical transition to thermoacoustic instability in a full-scale solid rocket motor

Cite as: Phys. Fluids **36**, 124127 (2024); doi: 10.1063/5.0246774
Submitted: 4 November 2024 · Accepted: 26 November 2024 ·
Published Online: 16 December 2024

Guanyu Xu (徐冠宇),[1] Bing Wang (王兵),[1] Peijin Liu (刘佩进),[2] and Yu Guan (关昱)[3,a)]

AFFILIATIONS

[1]School of Aerospace Engineering, Tsinghua University, Beijing, China
[2]Solid Rocket Propulsion National Laboratory, Northwestern Polytechnical University, Xi'an, China
[3]Department of Aeronautical and Aviation Engineering, The Hong Kong Polytechnic University, Kowloon, Hong Kong

[a)]Author to whom correspondence should be addressed: yu.guan@polyu.edu.hk

ABSTRACT

Thermoacoustic instability is a persistent problem frequently observed in various types of combustors, resulting in damaging consequences. However, our understanding of the dynamics in industrial combustors undergoing thermoacoustic instability, particularly in solid rocket motors, still remains limited. Data-driven precursors for thermoacoustic instability in such systems are also unknown. In this study, we use recurrence network measures and spectral entropy to characterize the dynamics of pressure data obtained from a full-scale solid rocket motor transitioning to thermoacoustic instability and design data-driven precursors for thermoacoustic instability. We show the scale-free nature of combustion noise and that the dynamical transition from combustion noise to thermoacoustic instability can be detected using two complex network measures: the average path length and average betweenness centrality. We calculate the spectral entropy in the frequency domain and find it more sensitive to detecting the dynamical transition and computationally cheap, which is promising for flexible use as a new precursor in thermoacoustic instability prediction. Our work highlights the feasibility of employing complex network measures and spectral entropy for precursors in solid rocket motors, paving a new path for using data-driven measures to early warning of thermoacoustic instability in solid rocket motors.

I. INTRODUCTION

Thermoacoustic instability is a problem that continues to affect various propulsion systems, despite attempts to eliminate it.[1] This instability arises from a specific phase connection between heat release rate fluctuation and pressure fluctuation.[2] When Rayleigh integral of these two oscillators yields a positive value, it establishes a positive feedback loop, amplifying their amplitudes.[3,4] The system undergoes linear and nonlinear growth stages until the amplitudes eventually reach their limits due to nonlinear damping, producing the thermoacoustic instability state.[5] The resulting high-amplitude pressure oscillations can cause performance degradation, structural fatigue, payload damage, or even catastrophic failure.[6,7] To address and prevent thermoacoustic instability, it is crucial to identify precursors by analyzing time series data of combustion noise prior to its onset.[8,9]

The study of precursors primarily focuses on combustion noise and intermittency, which serve as the primary dynamical states preceding thermoacoustic instability.[10,11] Combustion noise emerges from the unsteady combustion process, leading to volumetric expansion and compression of fluids in the vicinity of the flame region.[12] Distinguished from random oscillations, combustion noise exhibits deterministic behavior with chaotic nature, holding valuable insights into the evolution of instability.[13,14] Intermittency typically represents a transitional state during which a thermoacoustic system irregularly switches between two dynamical states.[15] For instance, before the occurrence of thermoacoustic instability, pressure fluctuations often exhibit a delayed recovery from external disturbances, commonly known as "critical slowing down."[16] Intermittency, as frequently emerging in the evolution of combustion instability, has consistently been a key area of focus. Nair *et al.*[17] investigated the transition from thermoacoustic instability to intermittency, leading to flame blowout, using a turbulent burner. Guan *et al.*[18] examined the intermittency pathway during the chaotic evolution process in a laminar flame burner. Capturing the underlying dynamics associated with the development of thermoacoustic instability from combustion noise and

intermittency at the earliest possible stage constitutes the core objective of early warning precursor research.

Both linear and nonlinear dynamic analysis methods can be employed to investigate combustion noise. Linear dynamic analysis methods provide valuable insights into the evolution patterns of thermoacoustic instability to a certain extent, and they have been employed to identify precursors of thermoacoustic instability based on pressure data. Pavithran and Sujith[19] conducted a study on thermoacoustic instability using the Rijke tube and successfully employed lag-1 autocorrelation analysis to detect precursors. In their investigation of a gas turbine engine test, An *et al.*[20] utilized variance, as well as the lag-1 autoregressive coefficient, to identify precursors for impending thermoacoustic instabilities. They observed that changes in these measures occurred several seconds before shifts in the amplitude of pressure oscillations. Bhattacharya *et al.*[21,22] employed a spectral-based method to calculate a scalar measure that effectively distinguishes between various working states of a simplified burner. This scalar metric indicates its practicality in identifying impending alterations associated with lean blow-out or thermoacoustic instability. However, when applied to industrial combustors, particularly rockets that frequently exhibit highly nonlinear behavior, linear dynamic analysis methods may struggle to uncover the intricate nature of the nonlinear dynamics involved. Flandro *et al.*[23] emphasized the potential risk of obtaining misleading results when attempting to analyze nonlinear dynamics using linear theory. The nonlinear dynamic analysis methods offer distinct advantages in extracting nonlinear dynamic characteristics from pressure data. Gotoda *et al.* and Domen *et al.* used translation error[24] and permutation entropy,[25] respectively, to detect thermoacoustic instability in gas-turbine model combustors. Nair *et al.* used recurrence quantification analysis and multifractal analysis to predict an impending thermoacoustic instability in a turbulent combustor and utilized the 0–1 test to quantify the state.[17,26,27] Song and Cha[28] explored the temporal Kurtosis of dynamic pressure signals to assess combustion stability quantitatively. Their findings suggest that temporal Kurtosis has the potential to function as an indicator of imminent severe combustion instability.

The thermoacoustic system is a typical complex system, comprising multiple interconnected elements, each exhibiting unique dynamic behaviors. The nonlinear interactions among these elements give rise to emergent behaviors. Consequently, studying a single element in isolation is inadequate for gaining a comprehensive understanding of the whole system. To address this, the complex network approach has been adopted. Among the various methods to construct complex networks, recurrence network is a representative approach.[29] Murugesan and Sujith[30] utilized complex network analysis to study the combustion noise produced by turbulent reacting flows, revealing the presence of scale invariance properties in the combustion noise. Gotoda *et al.*[31] utilized complex network analysis to develop an online detection strategy aimed at preventing thermoacoustic instability in a simplified turbulent combustor. Additionally, Kawano *et al.*[32] employed complex network analysis to investigate thermoacoustic instability in a single-element rocket model, with a particular emphasis on the spatiotemporal dynamics of high-frequency instability. Moreover, entropy serves as a measure of "disorder" in thermoacoustic systems. Its key benefit lies in its ability to quantitatively distinguish between regular dynamics and irregular noise. Additionally, it is particularly useful in engineering applications because it can be calculated quickly and efficiently.[33] Lee[34] investigated thermoacoustic instability in experimental and numerical systems. Based on fluctuations in heat release rate and pressure, the permutation entropy was employed to identify early warning signals of instability. Yao *et al.*[35] utilized a modified entropy algorithm based on spectral analysis to identify precursors of thermoacoustic instability in a simplified combustor.

The aforementioned studies primarily focused on laboratory combustors, such as swirl combustors and gas turbine models, to examine the dynamic characteristics and precursors of thermoacoustic instability. However, industrial combustors, particularly rocket motors, present challenges due to their highly nonlinear behavior, which adds complexity to the study of thermoacoustic instability.[36] Unlike gas turbines, both liquid and solid rocket motors exhibit more intricate dynamics,[37–39] including highly nonlinear steep front waveforms[40] and transitions between different types of period-k states.[41] Nevertheless, our current understanding of dynamics in industrial combustors, especially rocket motors, remains limited. Additionally, specific precursors of thermoacoustic instability for rocket motors are still lacking. To address these issues, this study employs two dynamic analysis methods—recurrence network (a representative complex network approach) and spectral entropy. These methods enable us to explore and comprehend the evolution of thermoacoustic instability dynamics in a full-scale solid rocket motor by examining both the geometric properties of the underlying attractor and entropy information in the frequency domain. The primary objectives of this study are twofold: 1) investigate and characterize the deterministic nature of combustion noise, an aspect that has not been extensively emphasized in solid rocket motors, and 2) detect precursors of impending thermoacoustic instabilities in a solid rocket motor.

The paper is structured as follows. Section II introduces the methodology of recurrence network analysis and spectral entropy. Section III A presents the experimental setup and provides an overview of the dynamics in the solid rocket motor. Sections III B and III C present the results obtained using recurrence network analysis and spectral entropy, respectively. Finally, Sec. IV concludes the study and provides a summary of the findings.

II. METHODOLOGY

A. Recurrence network

The complex network was developed using principles from graph theory and statistical physics.[42] In this framework, individual elements are represented as nodes, while the relationships between these elements are represented as links. As a result, these nodes and links form a complex network.[43] The number of links connected to a specific node is referred to as its degree, which quantifies the influence of that node within the complex network. Several methods can be employed to map pressure data onto a complex network, such as recurrence network,[29] correlation method,[44] cycle network,[45] and visibility graph.[46] In this study, the recurrence network is chosen for its ability to work effectively with low temporal sampling of the data. In comparison with other methods, the construction of a recurrence network requires less data, making it more advantageous for practical engineering applications. Consequently, a shorter rolling window can be used for sampling, facilitating the earlier detection of warning precursors. The recurrence network is constructed by analyzing the recurrence properties of trajectories in the phase space of time series data. The state points within the trajectories can be considered as nodes, and the

recurrence behavior of these state points is used to establish links. To quantify this recurrence property in the phase space, a recurrence matrix can be constructed as follows:

$$R_{i,j}(\varepsilon) = \Theta\big(\varepsilon - \|x_i - x_j\|\big), \tag{1}$$

where Θ represents the Heaviside function, while x_i and x_j denote distinct state points within the phase space. The recurrence threshold, denoted by ε, is determined as 20% of the attractor diameter based on previous findings in the literature.[17] The attractor diameter corresponds to the distance between the two farthest points in the phase space. $||.||$ represents the Euclidean norm, and $i, j = 1, 2, \ldots, N - (d-1)\tau$, where N is the number of points in the sampled time series. Here, τ represents the optimal time delay, and d is the minimum embedding dimension. The average mutual information (AMI) function[47] is employed to determine the optimal value of τ, while Cao's method[48] is utilized to compute d. If the Euclidean distance $|x_i - x_j|$ between two state points is less than the specified threshold ε, those state points are considered to have recurred. In the recurrence matrix, recurred state points are denoted by 1, while non-recurring points are represented by 0. To eliminate self-connections of the nodes, a Kronecker delta matrix ($\delta_{i,j}$) is subtracted from the recurrence matrix, $R_{i,j}(\varepsilon)$, resulting in the adjacency matrix as follows:

$$A_{i,j}(\varepsilon) = R_{i,j}(\varepsilon) - \delta_{i,j}, \tag{2}$$

where $\delta_{i,j} = 1$, if $i = j$, and $\delta_{i,j} = 0$, if $i \neq j$. The adjacency matrix only consists of values 0 and 1. A value of 0 indicates the absence of a link between the corresponding nodes, while a value of 1 signifies the presence of a link between the corresponding nodes. Consequently, the recurrence network is built by utilizing the nodes and links information derived from the adjacency matrix. It should be noted that the adjacency matrix doesn't provide directional information for the connections between nodes. Thus, the corresponding recurrence network is considered an undirected and unweighted network that effectively captures the geometric properties of the underlying attractor.

The average path length and average betweenness centrality of a recurrence network are helpful metrics for defining the system's transition between states.[49] They are being examined as potential indicators for detecting precursors to the thermoacoustic instability. The average shortest path between each pair of nodes in the network is represented by the average path length. The calculation of the average path length for any given network is performed as

$$L = \frac{1}{N(N-1)} \sum_{i,j=1, i\neq j}^{N} d_{(i,j)}, \tag{3}$$

where N represents the total number of nodes in the network. $d_{i,j}$ denotes the length of the shortest path between a pair of nodes (i, j), representing the minimum number of links required to connect node i with node j. It is important to note that disconnected nodes are not taken into account when computing the average path length.

Betweenness centrality measures the extent to which a particular node lies on the shortest paths between any pair of nodes in the network. It quantifies the proportion of such paths that include the node in question out of the total number of shortest paths. The calculation of the betweenness centrality for a node is as follows:

$$b_i = \sum_{j,k\in n, j\neq k} \frac{d_{(j,k)}(i)}{d_{(j,k)}}, \tag{4}$$

where $d_{j,k}$ represents the count of shortest paths between nodes j and k, while $d_{j,k}(i)$ indicates the number of those paths that pass through node i. Specifically, $d_{j,k}(i)$ denotes the quantity of shortest paths connecting nodes j and k that pass through node i. The concept of betweenness centrality enables the identification of bottleneck nodes or regions within the phase space that exhibit low density, acting as connectors between regions of high phase space density.

B. Spectral entropy

There are several methods available for computing signal entropy. In the time domain, one can consider metrics such as approximate entropy[50] and Shannon entropy.[51] In the frequency domain, spectral entropy[52] can be computed, offering the advantage of explicitly separating entropy contributions from specific frequency ranges. Many studies on identifying precursors of thermoacoustic instability primarily focus on utilizing information extracted from the time domain.[17,24–27] However, using the information extracted from the frequency domain can also yield excellent results in predicting thermoacoustic instability.[53] In this study, we employ spectral entropy based on the frequency domain to identify the precursor of thermoacoustic instability in solid rocket motors.

The computation process begins with the analysis of the signal spectrum. To obtain the spectrum, different spectral transformations can be employed, with the focus here being on the discrete Fourier transformation, as shown in Eq. (5). Through this transformation, the signal values, denoted as $x(t_i)$, at different moments t_i in a sampled time series, can be converted into an equal number of complex values across different frequencies, represented as $X(f_i)$

$$X(f_i) = \sum_{t_i} x(t_i) e^{-i2\Pi f_i t_i}. \tag{5}$$

The $X(f_i)$ can be efficiently computed based on the fast Fourier transform (FFT). Then, the power spectrum of the pressure data is analyzed using the Shannon entropy, which determines the spectral entropy within the specified frequency range $[f_1, f_2]$ for a given period of the signal. To obtain the power spectrum $P(f_i)$, $X(f_i)$ from the Fourier transform is squared

$$P(f_i) = X(f_i) \times X(f_i)^*, \tag{6}$$

where $X(f_i)^*$ represents the complex conjugate of the Fourier component $X(f_i)$, and the symbol $\times$ denotes multiplication.

Next, the power spectrum is normalized by determining the normalization constant, denoted as C_n, and applying it to obtain the normalized power spectrum $P_n(f_i)$. Finally, the sum of the normalized power spectrum within the specified frequency range $[f_1, f_2]$ is equal to one

$$\sum_{f_i=f_1}^{f_2} P_n(f_i) = C_n \sum_{f_i=f_1}^{f_2} P(f_i) = 1. \tag{7}$$

During the summing stage, the spectral entropy for the frequency range $[f_1, f_2]$ is calculated as the sum of the relevant terms

$$S[f_1,f_2] = \sum_{f_i=f_1}^{f_2} P_n(f_i)\log\left(\frac{1}{P_n(f_i)}\right). \quad (8)$$

The entropy value is subsequently normalized within a range from 1 (indicating the highest irregularity) to 0 (representing complete regularity). This normalization is achieved by dividing the entropy value by the factor $\log(N[f_1,f_2])$, where $N[f_1,f_2]$ corresponds to the total number of frequency components within the range $[f_1,f_2]$

$$S_N[f_1,f_2] = \frac{S[f_1,f_2]}{\log\left(N[f_1,f_2]\right)}. \quad (9)$$

The normalized spectral components $P_n(f_i)$ are subsequently transformed based on the Shannon function $(P_n(f_i) * \ln(1/P_n(f_i)))/\ln(N)$, to obtain the total spectral entropy.

III. RESULTS

A. Overview of the system dynamics

It is essential to acknowledge that triggering thermoacoustic instability in an actual full-scale solid rocket motor often involves typical nonlinear behavior. One notable aspect of this nonlinearity is the ground-to-air inconsistency.[54] This inconsistency implies the absence of instability during ground experiments, with the thermoacoustic instability only manifesting post-flight, potentially due to flight overload. To reproduce this post-flight instability on the ground, the rocket sled experiment proves to be an effective method.[55] In this experiment, a sufficiently long rail is positioned on the ground, and a sled securing the solid rocket motor can slide along this rail to simulate flight overload conditions.

Figure 1(a) shows the schematic representation of the rocket sled experiment, featuring a cylindrical combustion chamber. The combustor has a length of 2700 mm and a diameter of 300 mm. At the end of the combustion chamber, a convergent-divergent nozzle is connected. The solid propellant used is a mixture of ammonium perchlorate (AP) and hydroxyl-terminated polybutadiene (HTPB), combined with aluminum powder. The propellant grain adopts a wing-shaped structure, whereby the total burning surface area undergoes slight fluctuations during the recession of the burning surface, leading to variations in average pressure. However, the total burning rate area remains largely constant, with the average pressure sustained at 11.7 MPa until instability is triggered. The chamber temperature is estimated to be around 3500 K. The solid rocket motor is mounted on the sled that slides along the rail spanning over 1 km. A pressure transducer with a sampling rate of 19 200 Hz was positioned at the head end of the combustion chamber, allowing for the collection of over 70 data points per oscillation cycle.

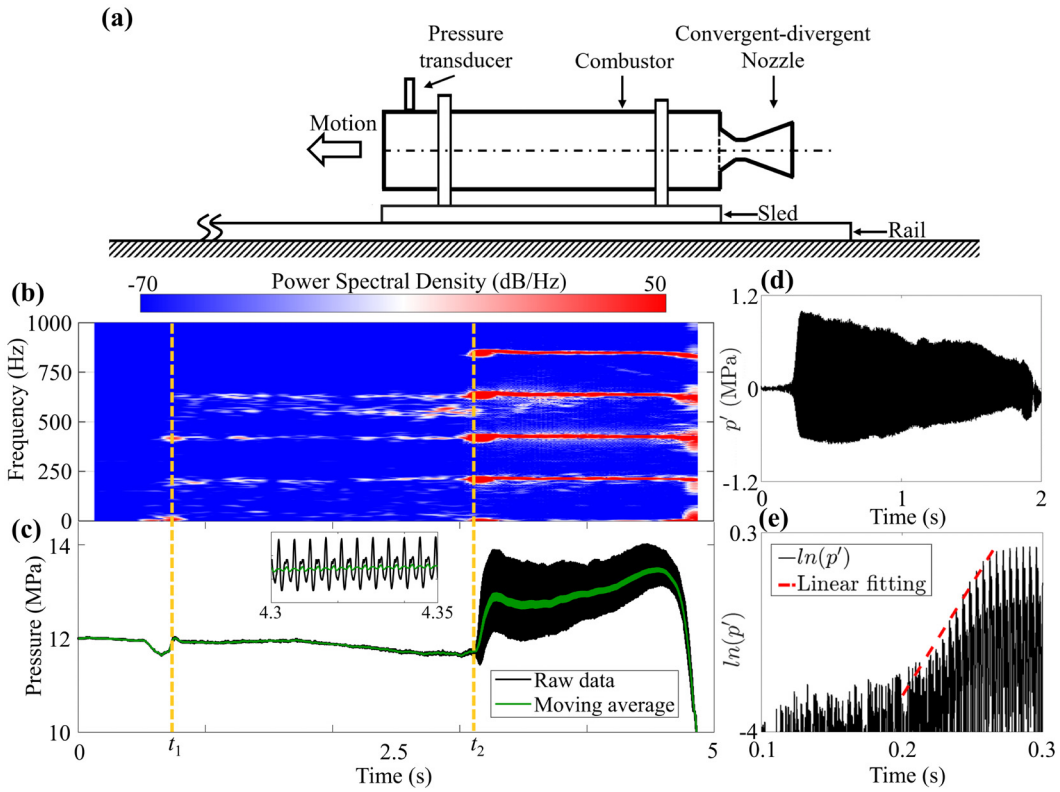

FIG. 1. (a) Diagram of the full-scale solid rocket motor used in this study.[41,56] (b) STFT diagram of pressure data. (c) Pressure evolution within the combustion chamber. The unsteady pressure is represented by the black line, and its average is represented by the green line. The orange dotted lines illustrate two triggering moments t_1 and t_2. While triggering at t_1 did not result in thermoacoustic instability, triggering at t_2 did. The thermoacoustic oscillations occur at $t_2 \approx 3.1$ s. The inset shows a zoom-in figure of unsteady pressure fluctuations. (d) Pressure data with moving average subtracted and time axis shifted (subtracted by 2.9 s) (i.e., pressure fluctuation p'). (e) Pressure fluctuation (p') on a log-linear plot, accompanied by a red dashed line representing the linear fitting.

It is noteworthy that even in rocket sled experiments, the reproduction of thermoacoustic instability can be somewhat unpredictable, given that the mechanism behind the thermoacoustic instability in solid rocket motors remains partially elusive. The mechanism governing thermoacoustic instability in solid rocket motors is notably complex because of the diverse gain and damping mechanisms stemming from the non-constant volume combustion process, heterogeneous propellant composition, and metal particle combustion and agglomeration. Moreover, conducting rocket sled experiments is both costly and dangerous. Regrettably, we have thus far acquired only a single set of experimental data on thermoacoustic instability. Nonetheless, these data effectively capture the thermoacoustic instability phenomenon in a real solid rocket motor experiencing flight overload conditions, a scenario that is typical and valuable. Further exploitation of this dataset for more advanced data analysis naturally holds significant benefits.

Figure 1(c) displays the pressure evolution within the combustion chamber. The inset of Fig. 1(c) provides a zoomed-in view of the unsteady pressure fluctuations. The black line represents the unsteady pressure, while the green line corresponds to the average pressure using a moving window of 0.005 s. These curves illustrate the complete process, encompassing the triggering, growth, saturation, and decay of the oscillations. A triggering event is defined as a sudden change in pressure amplitude, occurring at $t_1 \approx 0.65$ s and $t_2 \approx 3.1$ s. While it is challenging to provide a definitive explanation for the cause of thermoacoustic instability due to limitations in measurement technology, the overload from the solid rocket's acceleration is likely the main factor. The triggering event at t_1 did not lead to thermoacoustic instability, as the pressure amplitude quickly decayed. During the early phase of the solid rocket motor's operation, the propellant grain generally retains its wing-shaped structure, which provides significant structural damping and effectively suppresses weak coupling oscillations before the system reaches the instability boundary. However, the triggering event at t_2 did result in thermoacoustic instability. In the later phase of operation, as the burning surface recedes, the propellant grain transitions to an inner-hole structure. This change reduces structural damping, increasing the system's susceptibility to thermoacoustic instability.

Figure 1(b) displays the short-time Fourier transform (STFT) result of the pressure time series data. In the stable state, the frequency distribution appears dispersed, with a noticeable protrusion observed near the thermoacoustic instability boundary. In contrast, during an unstable state, the frequency distribution is characterized by a few distinct and sharp peaks, indicating a shift from disorder to order. Notably, the coexistence of the fundamental frequency and its multiple harmonics is a typical nonlinear phenomenon in solid rocket motors, caused by energy transfer from low-order acoustic modes to high-order ones. Higher frequencies, however, experience greater nonlinear damping, leading to their attenuation. To investigate system dynamics, we extract the data from this two-second window, subtract its moving average, and shift its time axis (subtracted 2.9 s) to receive a dataset for analysis $\{p'(t)\}_{t=0}^{t=2s}$, as shown in Fig. 1(d). During the initial growth of these oscillations, which begins at $t \approx 0.2$ s, the same driving mechanism for producing thermoacoustic oscillations also causes a DC shift in the mean pressure.[54] Figure 1(e) focuses on this initial growth stage by showing the pressure with its moving average subtracted out. In this log-linear graph, it is evident that the oscillation amplitude exhibits linear growth, indicating exponential growth at a rate of $51.54\,s^{-1}$. Subsequently, the pressure oscillation reaches a saturation point as the system's damping and gain achieve a balance. Finally, the pressure oscillation decays as the solid propellant is depleted. For a more comprehensive exploration of the dynamic characteristics, interested readers are directed to the relevant literature.[41,56]

B. Complex network analysis

Initially, pressure data of the combustion noise, thermoacoustic instability, and intermittency before the two triggering events are sampled using a window of 0.1 s. This window length is chosen to ensure enough sensitivity to dynamic changes and to capture sufficient dynamic characteristics. The classification of the three states is based on the STFT results shown in Fig. 1(b). The frequency distribution of combustion noise is relatively dispersed, whereas the frequency distribution for thermoacoustic instability is concentrated, exhibiting several distinct peaks. In the case of intermittency, the frequency spectrum starts to concentrate due to critical slowing down. Additional details regarding the classification of these states can be found in our previous work.[57] Subsequently, recurrence network analysis is conducted on the sampled data, and the Gephi software is used to visualize the network topology, as depicted in Figs. 2(a)–2(f). Gephi is an open source software for exploring and manipulating networks.[58] In Figs. 2(a)–2(f), nodes are represented by dots of varying colors and sizes, indicating their respective degree levels. The length of a link is not particularly important; what truly matters is the number of links. A node with more links has a higher degree, meaning it connects to more elements. This higher degree indicates that the element carries greater weight and has a stronger influence on the overall system.

Figure 2(c) illustrates the network topology of combustion noise (2.5–2.6 s). It can be observed that the degrees span a range from low to medium to high, with no discernible regular topology evident. In comparison, Fig. 2(a) demonstrates the network topology for completely random signals. In this case, the majority of nodes exhibit high degree. This observation confirms that the pressure data from combustion noise differ from random signals. It indicates that noise is not synonymous with randomness; rather, it possesses a certain deterministic nature.[26] In solid rocket motors, the combustion of inhomogeneous propellants generates many random hot spots due to the irregular distribution of oxidizer particles (AP) in the binder (HTPB). The volume expansion caused by these hot spots creates random perturbations, which are the source of the unpredictable component of combustion noise. These perturbations travel through the combustion chamber at the speed of sound and reflect off the chamber walls, forming standing waves. These standing waves are the basis of the deterministic component of combustion noise. It is important to note that when heat and acoustics are not coupled, the standing waves are weak, with very low amplitudes. The combination of random perturbations from hot spots and standing waves gives the signal a disordered appearance, resembling a random signal. However, a truly random signal is different, lacking any ordered components.

Figures 2(d) and 2(e) represent the network topology during the first intermittency (0.55–0.65 s) and the second intermittency (3–3.1 s) preceding the two triggering events, respectively. The proportion of high-degree nodes is noticeably reduced, with a concentration of low-degree nodes at the center of the graph. Notably, repetitive ring structures begin to emerge on the periphery, indicating an increase in system orderliness. Gephi operates with a mechanism where nodes repel each other, creating a repulsive force, while the connections between

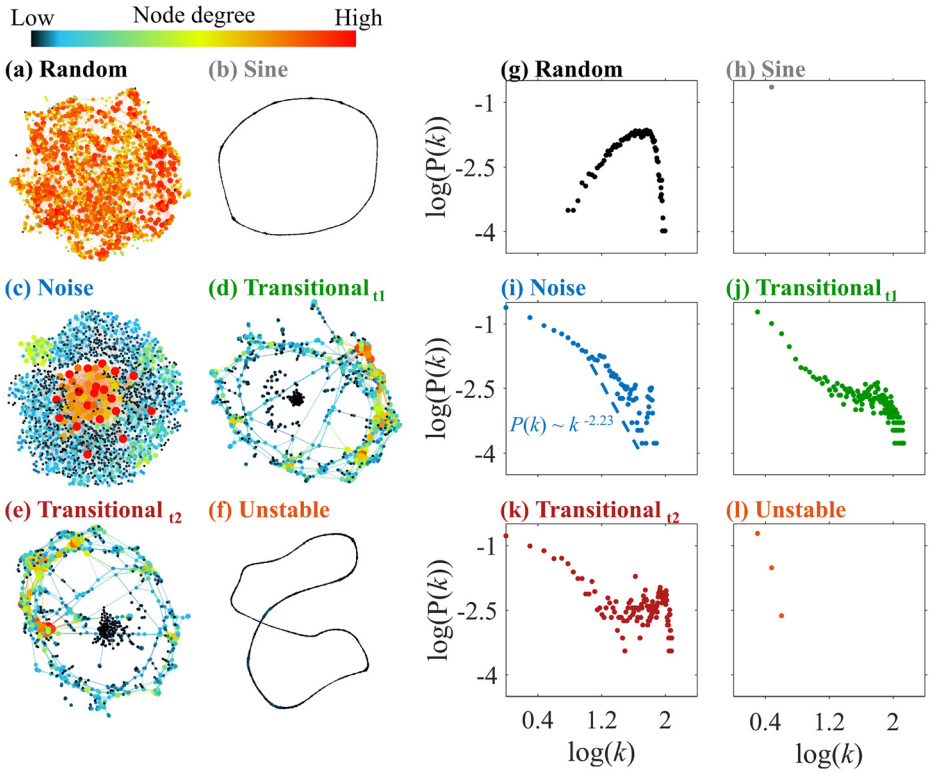

FIG. 2. (a)–(f):Network topologies corresponding to different states. (c) Combustion noise, (e) thermoacoustic instability, and (d) and (e) intermittency before the two triggering events. Additionally, (a) and (b) show the network topologies for random signal and sinusoidal signal, respectively, for comparison. (g)–(l) Degree distributions for various states: (i) combustion noise, (l) thermoacoustic instability, and (j) and (k) intermittency before the two triggering events. Additionally, (g) and (h) show the degree distributions for random signal and sinusoidal signal, respectively, for comparison.

nodes act as a pulling force. In Figs. 2(d) and 2(e), middle-degree nodes exhibit an approximate circular formation due to the interplay of these two forces. Low-degree nodes (black symbols), lacking links (pulling forces) with other nodes, cluster in the center due to the repulsive effect of the ring structure. In Fig. 2(c), high-degree nodes, which have more links, form a central cluster under the influence of strong pulling forces, while the remaining low-degree nodes are distributed around the cluster due to its repulsive effect. The similarity in dynamical states observed during the two triggering events highlights the common characteristics of the transition state in the evolution of thermoacoustic instability. In this state, the emergence of weak coupling between heat and acoustic increases the amplitude of the ordered component in the combustion noise, which leads to changes in the topological structure of the complex network and the appearance of ordered patterns. However, this weak coupling is fragile and can be easily disrupted by system damping. This indicates that while the transition state is necessary for the development of thermoacoustic instability, it is not sufficient on its own. In practice, the key to early prediction of thermoacoustic instability lies in accurately identifying the transition state and implementing measures to disrupt this weak thermoacoustic coupling.

Figure 2(f) presents the network topology for thermoacoustic instability (3.3–3.4 s), exhibiting good repeatability with generally low node degrees. Due to the periodicity of the oscillation, the system has entered an ordered limit cycle. However, this topology deviates from a typical ring structure and appears distorted. In a solid rocket motor, the transfer of energy among multiple acoustic modes leads to period-k oscillation in the limit cycle, resulting in a more complex network structure. For comparison, Fig. 2(b) demonstrates an artificially constructed single-mode sinusoidal oscillation with a constant amplitude, where a typical ring structure can be observed.

The measures derived from the recurrence network are further examined, particularly focusing on the distribution of node degrees denoted as k. In this context, we utilize $P(k)$ to denote the proportion occupied by nodes with a degree of k. Figures 2(g)–2(l) illustrate the relationship between $\log(k)$ and $\log(P(k))$, which aligns with the pressure data corresponding to (a)–(e). In Fig. 2(i), the variation of the $\log(k)$-$\log(P(k))$ from combustion noise is depicted and the power law can be observed, represented as $P(k) = k^{-\gamma}$. The value of γ is calculated as 2.23, falling between 2 and 3, indicating the scale-free topology of the network.[59,60] A scale-free property indicates that the signal exhibits fractal characteristics. A fractal is an object whose smaller parts resemble, either exactly or approximately, the structure of the entire object. In other words, the signal demonstrates a degree of self-similarity, reflecting the repeating patterns of fractals across different observational scales. This property can be quantitatively analyzed using a power law. Notably, this is the first observation of scale-free behavior in the combustion noise of a solid rocket motor. It is important to note that in theory, a power law distribution should not have any outliers, and the entire distribution should conform to the power law. However, in practical systems, there may be some outliers present. Therefore, if at least 80% of the $\log(k)$-$\log(P(k))$ points adhere to a power law, we consider the overall degree distribution to follow a power law in our current study. Figure 2(g) displays the degree distribution of random signals, revealing a significant portion that deviates from the power law. Regarding intermittency, Figs. 2(j) and 2(k)

demonstrate a substantial decrease in the portion of the degree distribution that adheres to the power law when compared to Fig. 2(i). This finding further confirms the dynamic similarity observed near the thermoacoustic instability boundary. In the case of the sinusoidal signal depicted in Fig. 2(h), the periodic sinusoidal oscillation results in all nodes having the same degree, resulting in a concentrated degree distribution centered around one node. For the state of thermoacoustic instability illustrated in Fig. 2(l), the degree distribution also exhibits a concentrated pattern due to limit cycle oscillation. However, due to the highly nonlinear behavior observed in solid rocket motors, the degree distribution is not solely concentrated on one node but rather on several nodes.

The average path length (L_c) and average betweenness centrality (B_c) are derived from the recurrence network and are used as measures to estimate the proximity to thermoacoustic instability in a solid rocket motor, depicted by red and blue lines in Fig. 3. It should be noted that all quantities have been normalized for convenient comparison of the changing trends among different precursors. The maximum average path length is observed during combustion noise, attributable to reduced recurrences in the phase space, consequently resulting in longer shortest paths between nodes. At time t_1, there is an abrupt decrease in the average path length, reaching a local minimum of 0.62. Therefore, we set this value as the threshold. At time t_2, there is another abrupt drop in the average path length, reaching the threshold. When pressure oscillation becomes saturated, the average path length remains below the threshold due to the shorter shortest paths between nodes resulting from higher degrees. It is important to highlight that when the warning signal reaches the threshold, it signifies the system's proximity to the instability boundary, as seen at time t_1. This does not guarantee instability will occur, as the system's damping may potentially suppress instability. Nonetheless, offering a warning signal when the system nears the unstable boundary fulfills our criteria, enabling us to promptly implement suppression measures and maintain a significant stability margin.

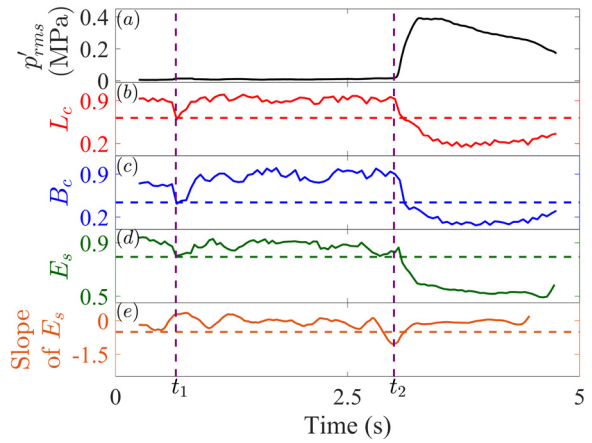

FIG. 3. The black, red, blue, green, and orange lines show the temporal variation of the following variables: (a) root mean square of pressure fluctuation (p'_{rms}), (b) average path length (L_c), (c) average betweenness centrality (B_c), (d) spectral entropy evolution (E_s), and (e) slope of spectral entropy, respectively. The horizontal dotted lines represent thresholds of different warning precursors of thermoacoustic instability, while the vertical dotted lines indicate two triggering moments.

The average betweenness centrality demonstrates a comparable trend to the average path length. It is evident that higher values of betweenness centrality are observed during combustion noise. The threshold is arbitrary set at 0.44. Notably, at times t_1 and t_2, the average betweenness centrality exhibits a substantial decrease and reaches the threshold. The betweenness centrality remains low during thermoacoustic instability. Betweenness centrality can be employed to identify regions with low phase space density, enabling the distinction of regions with high phase space density. Higher levels of betweenness centrality suggest that the attractor has substantial local fragmentation.[61] Due to the evident periodic properties of thermoacoustic instability, the regions with high phase space density are uniformly distributed. Consequently, the betweenness centrality during thermoacoustic instability remains low.

In this section, we employ recurrence network analysis to examine the complete cycle of thermoacoustic instability evolution. The visualizing network topology can uncover the geometric properties of the underlying attractor, allowing to characterize various dynamic states. Through the analysis of $\log(k)$-$\log(P(k))$, we reveal the scale-free nature of combustion noise, emphasizing its deterministic characteristics. Furthermore, we find that measures such as average path length and betweenness centrality in the recurrence network serve as useful indicators for defining the system's transitions between states and have the potential to predict thermoacoustic instability.

C. Spectral entropy

Compared to the recurrence network, which analyzes system dynamics in the time domain to provide precursors, spectral entropy offers an alternative indicator of thermoacoustic instability based on the frequency domain. In thermoacoustic systems, spectral entropy approximates 1 during the combustion noise state, as no distinct frequency peak exists, and approaches 0 for the limit cycle state, characterized by several sharp frequency peaks. In this study, the frequency range for estimating spectral entropy is limited from 10 to 1000 Hz, excluding the influence of low-frequency noise and focusing on the first four harmonics (from f_n to $4f_n < 1000$ Hz, $f_n \approx 210$ Hz). The complete dataset [presented in Fig. 1(c) with moving average subtracted] is divided into 95% overlapping sliding windows of 3840 data points (0.2 s). Spectral entropy (E_s) is calculated for each window and subsequently normalized. As depicted by the green line in Fig. 3, spectral entropy exhibits a significant drop (from 0.93 to 0.80) at t_1, resulting in a local minimum. As oscillations dampen and the combustion process progresses, spectral entropy returns to a value around 0.9. As time gradually approaches the second triggering event, p'_{rms} steadily increases, leading to another notable drop in spectral entropy at $t \approx 2.85$ s, which precedes the triggering event at $t_2 \approx 3.1$ s. When the pressure amplitude saturates, spectral entropy stabilizes around 0.50 but does not approach 0. This occurrence can be attributed to the presence of multiple dominant acoustic modes within the system and the persistent noise, which prevents the spectral entropy from approaching 0. The slope of the spectral entropy was calculated using a moving window of 30 data points, with the slopes averaged within each window, as shown in Fig. 3(e). This approach helps us to visualize the trend of spectral entropy more intuitively. For both combustion noise and thermoacoustic instability states, the slope of spectral entropy fluctuates around zero. However, near time points t_1 and t_2, the slope shows

a sharp decline, indicating an impending significant change in spectral entropy.

We established thresholds of 0.79 for spectral entropy and −0.5 for its slope, corresponding to their respective local minima. Compared to average path length and average betweenness centrality, the combination of spectral entropy and its slope offers an earlier indication of thermoacoustic instability. The times at which L_c and B_c reach their thresholds are 3.14 and 3.15 s, respectively. In contrast, the slope of E_s reaches its threshold at 2.87 s, which is 0.27 s earlier than L_c and 0.28 s earlier than B_c. This time difference is likely to increase when processing real-time pressure signals due to the computational inefficiency of the complex network approach. This early detection capability assists operators in implementing essential procedures for controlling and preventing thermoacoustic instabilities.[62,63] Using data-driven precursors to quantify the proximity to instability onset offers significant benefits. (i) It allows us to focus on uncovering the underlying physical mechanisms during the critical transition, marked by large variations in precursor values, from which the system eventually evolves into a high-amplitude limit cycle. This approach helps target key issues more precisely. (ii) Additionally, the developed precursors can be adapted to other types of rocket engines, such as hybrid rocket engines[64–66] and liquid rocket engines,[67,68] enabling the implementation of effective control measures to suppress combustion instability. For example, to actively control thermoacoustic instability in liquid rocket motors, the fuel-to-oxidizer equivalence ratio can be adjusted in real time to alter the heat release when an early warning is detected. This adjustment breaks the coupling between heat release and acoustic oscillations, effectively preventing the development of thermoacoustic instability. Moreover, when comparing with average path length and average betweenness centrality, spectral entropy offers simpler calculation steps and quicker results. Obtaining average path length and average betweenness centrality involves multiple transformations, making the process more challenging. Due to the superior advance and computational efficiency of E_s based on spectral entropy, it is more suitable for practical engineering applications, potentially enabling real-time online prediction of thermoacoustic instability.

In this section, we conducted tests using spectral entropy to quantify the proximity of the onset of thermoacoustic instabilities in a solid rocket motor. The findings reveal that by monitoring the slope of the linear fitting line of spectral entropy, we can identify the critical transition early before the fully excited thermoacoustic instability. Meanwhile, p'_{rms} does not exhibit significant variations, suggesting that the spectral entropy is sensitive to changes in system states. Moreover, the faster calculation speed of spectral entropy enhances its efficiency, rendering it more valuable for engineering applications, which should also be considered for those gas turbine combustors where rich nonlinear dynamics were reported.[69–73]

IV. CONCLUSIONS

In this study, we study the thermoacoustic instability in an unstable solid rocket motor using recurrence network analysis and spectral entropy. We first uncover intricate dynamics during the transition from combustion noise to thermoacoustic instability. We show the first experimental evidence of the scale-free behavior of combustion noise in a solid rocket motor. We analyze characteristic geometric properties of the networks, indicative of combustion noise, intermittency, and thermoacoustic instability. We then assess the predictive capability of two recurrence network metrics—average path length and average betweenness centrality—as well as spectral entropy. Our results indicate that spectral entropy offers higher sensitivity to dynamical transitions and is computationally efficient. Based on our findings in this study, it is suggested that (1) the pressure oscillations in a full-scale solid rocket motor can display similar network properties, potentially strengthening the link between thermoacoustic instabilities in solid rocket motors and other combustion systems; and (2) recurrence network metrics and spectral entropy could serve as early warning signals for developing control strategies and online prediction tools. Data-driven methods are expected to play an increasingly crucial role in studying thermoacoustic instability, as advancements in both hardware and algorithms enable deeper insights exploited from existing experimental data and high-fidelity simulations.[74,75] In thermoacoustic systems, the coupling between pressure fluctuations and heat release fluctuations causes the heat release signal to often exhibit dynamics similar to those of the pressure signal, enabling a potential early detection of thermoacoustic instability. While heat release signals are not available in rocket sled experiments due to current monitoring limitations, they could theoretically be used for early predictions in such cases as well. This potential application holds significant value for other systems where heat release signals can be measured.

ACKNOWLEDGMENTS

G.X. was supported by the Postdoctoral Fellowship Program (Grade C) of the China Postdoctoral Science Foundation (Grant No. GZC20231240) and the China Postdoctoral Science Foundation (Grant No. 2024M751666). Y.G. was supported by the National Natural Science Foundation of China (Grant No. 52306166).

AUTHOR DECLARATIONS

Conflict of Interest

The authors have no conflicts to disclose.

Author Contributions

Guanyu Xu: Writing – review & editing (equal). **Bing Wang:** Writing – review & editing (equal). **Peijin Liu:** Writing – review & editing (equal). **Yu Guan:** Writing – review & editing (equal).

DATA AVAILABILITY

The data that support the findings of this study are available from the corresponding author upon reasonable request.

REFERENCES

[1]R. I. Sujith and S. A. Pawar, *Thermoacoustic Instability: A Complex Systems Perspective* (Springer, 2021).
[2]F. Culick and P. Kuentzmann, "Unsteady motions in combustion chambers for propulsion systems," Tech. Rep. (DTIC Document, 2006).
[3]G. Kelsall and C. Troger, "Prediction and control of combustion instabilities in industrial gas turbines," Appl. Therm. Eng. **24**, 1571–1582 (2004).
[4]T. Liu, J. Li, S. Zhu, and L. Yang, "Determination of the heat conduction transfer function within the thermoacoustic instability limit cycle in a Rijke tube," Appl. Therm. Eng. **206**, 118084 (2022).
[5]K. Moon, D. Bae, and K. T. Kim, "Modal dynamics of self-excited thermoacoustic instabilities in even and odd numbered networks of lean-premixed combustors," Combust. Flame **255**, 112928 (2023).

[6]F. Culick, "Combustion instabilities in solid propellant rocket motors," Tech. Rep. (DTIC Document, 2004).
[7]X. Liang, Z. Wang, L. Ji, L. Yang, and J. Li, "Comparisons between the disturbances in chemiluminescence and heat release rate from acoustically perturbed partially premixed and diffusion flames," Phys. Fluids **36**, 023621 (2024).
[8]C. Tao, R. Sun, Y. Wang, L. Zhang, J. Ye, and S. Liang, "The effects of parameter settings on triggering time and climb rate during lean-premixed combustion thermoacoustic oscillations," Appl. Sci. **14**, 806 (2024).
[9]C. Tao and H. Zhou, "Effects of superheated steam on combustion instability and NOx emissions in a model lean premixed gas turbine combustor," Fuel **288**, 119646 (2021).
[10]D. Zhao, C. Ji, and H. Huang, "Thermal fluid dynamics and control in aerospace" (2023).
[11]U. Sengupta, G. Waxenegger-Wilfing, J. Martin, J. Hardi, and M. P. Juniper, "Forecasting thermoacoustic instabilities in liquid propellant rocket engines using multimodal Bayesian deep learning," Int. J. Spray Combust. Dyn. **14**, 218–228 (2022).
[12]I. C. Waugh and M. P. Juniper, "Triggering in a thermoacoustic system with stochastic noise," Int. J. Spray Combust. Dyn. **3**, 225–241 (2011).
[13]Y. Liao, Y. Guan, P. Liu, K. Moon, and K. T. Kim, "Low-order modeling of collective dynamics of four ring-coupled turbulent thermoacoustic oscillators," Nonlinear Dyn. **112**, 6897 (2024).
[14]G. Waxenegger-Wilfing, U. Sengupta, J. Martin, W. Armbruster, J. Hardi, M. P. Juniper, and M. Oschwald, "Early detection of thermoacoustic instabilities in a cryogenic rocket thrust chamber using combustion noise features and machine learning," Chaos **31**, 063128 (2021).
[15]M. P. Juniper, "Sensitivity and nonlinearity of thermoacoustic oscillations," Annu. Rev. Fluid Mech. **50**, 661–689 (2018).
[16]M. Scheffer, J. Bascompte, W. A. Brock, V. Brovkin, S. R. Carpenter, V. Dakos, H. Held, E. H. Van Nes, M. Rietkerk, and G. Sugihara, "Early-warning signals for critical transitions," Nature **461**, 53–59 (2009).
[17]V. Nair, G. Thampi, and R. I. Sujith, "Intermittency route to thermoacoustic instability in turbulent combustors," J. Fluid Mech. **756**, 470–487 (2014).
[18]Y. Guan, V. Gupta, and L. K. B. Li, "Intermittency route to self-excited chaotic thermoacoustic oscillations," J. Fluid Mech. **894**, R3 (2020).
[19]I. Pavithran and R. I. Sujith, "Effect of rate of change of parameter on early warning signals for critical transitions," Chaos **31**, 013116 (2021).
[20]Q. An, A. M. Steinberg, S. Jella, G. Bourque, and M. Füri, "Early warning signs of imminent thermoacoustic oscillations through critical slowing down," J. Eng. Gas Turbines Power **141**, 054501 (2019).
[21]C. Bhattacharya, J. O'Connor, and A. Ray, "Data-driven detection and early prediction of thermoacoustic instability in a multi-nozzle combustor," Combust. Sci. Technol. **194**, 1481–1512 (2022).
[22]C. Bhattacharya, S. De, A. Mukhopadhyay, S. Sen, and A. Ray, "Detection and classification of lean blow-out and thermoacoustic instability in turbulent combustors," Appl. Therm. Eng. **180**, 115808 (2020).
[23]G. A. Flandro, S. Malhotra, and D. Garza, "Nonlinear combustion instability data reduction," in Proceeding of the 32nd AIAA/ASME/SAE/ASEE Joint Propulsion Conference and Exhibit. AIAA Paper (1996).
[24]H. Gotoda, Y. Shinoda, M. Kobayashi, Y. Okuno, and S. Tachibana, "Detection and control of combustion instability based on the concept of dynamical system theory," Phys. Rev. E **89**, 022910 (2014).
[25]S. Domen, H. Gotoda, T. Kuriyama, Y. Okuno, and S. Tachibana, "Detection and prevention of blowout in a lean premixed gas-turbine model combustor using the concept of dynamical system theory," Proc. Combust. Inst. **35**, 3245–3253 (2015).
[26]V. Nair, G. Thampi, S. Karuppusamy, S. Gopalan, and R. I. Sujith, "Loss of chaos in combustion noise as a precursor of impending combustion instability," Int. J. Spray Combust. Dyn. **5**, 273–290 (2013).
[27]V. Nair and R. I. Sujith, "Multifractality in combustion noise: Predicting an impending combustion instability," J. Fluid Mech. **747**, 635–655 (2014).
[28]W. J. Song and D. J. Cha, "Temporal kurtosis of dynamic pressure signal as a quantitative measure of combustion instability," Appl. Therm. Eng. **104**, 577–586 (2016).
[29]R. Jacob, K. P. Harikrishnan, R. Misra, and G. Ambika, "Uniform framework for the recurrence-network analysis of chaotic time series," Phys. Rev. E **93**, 012202 (2016).
[30]M. Murugesan and R. I. Sujith, "Combustion noise is scale-free: Transition from scale-free to order at the onset of thermoacoustic instability," J. Fluid Mech. **772**, 225–245 (2015).
[31]H. Gotoda, H. Kinugawa, R. Tsujimoto, S. Domen, and Y. Okuno, "Characterization of combustion dynamics, detection, and prevention of an unstable combustion state based on a complex-network theory," Phys. Rev. Appl. **7**, 044027 (2017).
[32]K. Kawano, H. Gotoda, Y. Nabae, Y. Ohmichi, and S. Matsuyama, "Complex-network analysis of high-frequency combustion instability in a model single-element rocket engine combustor," J. Fluid Mech. **959**, A1 (2023).
[33]S. L. Ding, B. Guo, Z. T. Liu, J. J. Liu, P. Tunestål, E. Z. Song, and C. Cui, "Analysis of the fractal characteristics for combustion instability in a premixed natural gas engine," Appl. Therm. Eng. **233**, 121177 (2023).
[34]M. Lee, "Early warning detection of thermoacoustic instability using three-dimensional complexity-entropy causality space," Exp. Therm. Fluid Sci. **130**, 110517 (2022).
[35]Y. Li, C. Hu, Y. Shen, B. Han, J. Yang, and G. Xu, "A new methodology for early detection of thermoacoustic combustion oscillations based on permutation entropy," J. Therm. Sci. **32**, 2310–2320 (2023).
[36]X. Wang, Y. H. Chang, Y. Li, V. Yang, and Y. H. Su, "Surrogate-based modeling for emulation of supercritical injector flow and combustion," Proc. Combust. Inst. **38**, 6393–6401 (2021).
[37]F. Culick, "Internal aerodynamics in solid rocket propulsion," Tech. Rep. (NATO, 2002).
[38]G. Xu, B. Wang, B. Jin, Z. Wang, and P. Liu, "Numerical study of triggered thermoacoustic instability driven by linear and nonlinear combustion response in a solid rocket motor," Phys. Fluids **36**, 034110 (2024).
[39]G. Xu, P. Liu, W. Ao, Z. Wang, and B. Jin, "Numerical investigation of thermoacoustic instability caused by small disturbance in a solid rocket motor," Aerosp. Sci. Technol. **113**, 106678 (2021).
[40]P. Kasthuri, I. Pavithran, S. Pawar, R. Sujith, R. Gejji, and W. Anderson, "Dynamical systems approach to study thermoacoustic transitions in a liquid rocket combustor," Chaos **29**, 103115 (2019).
[41]Y. Guan, P. Liu, B. Jin, V. Gupta, and L. K. B. Li, "Nonlinear time-series analysis of thermoacoustic oscillations in a solid rocket motor," Exp. Therm. Fluid Sci. **98**, 217–226 (2018).
[42]S. H. Strogatz, "Exploring complex networks," Nature **410**, 268–276 (2001).
[43]J. Ladyman, J. Lambert, and K. Wiesner, "What is a complex system?," Euro. J. Philos. Sci. **3**, 33–67 (2013).
[44]Y. Yang and H. Yang, "Complex network-based time series analysis," Phys. A **387**, 1381–1386 (2008).
[45]Y. Zou, R. V. Donner, J. F. Donges, N. Marwan, and J. Kurths, "Identifying complex periodic windows in continuous-time dynamical systems using recurrence-based methods," Chaos **20**, 043130 (2010).
[46]L. Lacasa, B. Luque, F. Ballesteros, J. Luque, and J. C. Nuno, "From time series to complex networks: The visibility graph," Proc. Natl. Acad. Sci. U. S. A. **105**, 4972–4975 (2008).
[47]A. M. Fraser and H. L. Swinney, "Independent coordinates for strange attractors from mutual information," Phys. Rev. A **33**, 1134 (1986).
[48]L. Cao, "Practical method for determining the minimum embedding dimension of a scalar time series," Phys. D **110**, 43–50 (1997).
[49]Y. Zou, R. V. Donner, N. Marwan, J. F. Donges, and J. Kurths, "Complex network approaches to nonlinear time series analysis," Phys. Rep. **787**, 1–97 (2019).
[50]S. M. Pincus, "Approximate entropy as a measure of system complexity," Proc. Natl. Acad. Sci. U. S. A. **88**, 2297–2301 (1991).
[51]J. Lin, "Divergence measures based on the Shannon entropy," IEEE Trans. Inform. Theory **37**, 145–151 (1991).
[52]B. Bein, "Entropy," Best Pract. Res., Clin. Anaesthesiol. **20**, 101–109 (2006).
[53]A. Banerjee, I. Pavithran, and R. Sujith, "Early warnings of tipping in a non-autonomous turbulent reactive flow system: Efficacy, reliability, and warning times," Chaos **34**, 013113 (2024).
[54]G. A. Flandro, S. R. Fischbach, and J. Majdalani, "Nonlinear rocket motor stability prediction: Limit amplitude, triggering, and mean pressure shift," Phys. Fluids **19**, 094101 (2007).
[55]S. Walia, V. Satya, S. Malik, S. Chander, S. Devi, and A. Sharma, "Rocket sled based high speed rail track test facilities: A review," Def. Sci. J. **72**, 182–194 (2022).

[56]G. Xu, B. Wang, Y. Guan, Z. Wang, and P. Liu, "Early detection of Hopf bifurcation in a solid rocket motor via transfer learning," Phys. Fluids **35**, 124113 (2023).
[57]G. Xu, B. Wang, Y. Guan, Z. Wang, and P. Liu, "Early detection of thermoacoustic instability in a solid rocket motor: A generative adversarial network approach with limited data," Appl. Energy **373**, 123776 (2024).
[58]M. Bastian, S. Heymann, and M. Jacomy, "Gephi: An open source software for exploring and manipulating networks," in *Proceedings of the International AAAI Conference on Web and Social Media* (AAAI, 2009), Vol. 3, pp. 361–362.
[59]A. Barabási and R. Albert, "Emergence of scaling in random networks," Science **286**, 509–512 (1999).
[60]Y. Guan, Y. Zhu, Z. Yang, B. Yin, V. Gupta, and L. K. B. Li, "Multifractality and scale-free network topology in a noise-perturbed laminar jet," J. Fluid Mech. **972**, A6 (2023).
[61]R. V. Donner, Y. Zou, J. F. Donges, N. Marwan, and J. Kurths, "Recurrence networks—a novel paradigm for nonlinear time series analysis," New J. Phys. **12**, 033025 (2010).
[62]Y. Guan, W. He, M. Murugesan, Q. Li, P. Liu, and L. K. B. Li, "Control of self-excited thermoacoustic oscillations using transient forcing, hysteresis and mode switching," Combust. Flame **202**, 262–275 (2019).
[63]Y. Guan, V. Gupta, K. Kashinath, and L. K. B. Li, "Open-loop control of periodic thermoacoustic oscillations: Experiments and low-order modelling in a synchronization framework," Proc. Combust. Inst. **37**, 5315–5323 (2019).
[64]K. S. Park and C. Lee, "Low frequency instability in laboratory-scale hybrid rocket motors," Aerosp. Sci. Technol. **42**, 148–157 (2015).
[65]H. Tian, Y. l Li, C. Li, and X. Sun, "Regression rate characteristics of hybrid rocket motor with helical grain," Aerosp. Sci. Technol. **68**, 90–103 (2017).
[66]N. A. Davydenko, R. G. Gollender, A. M. Gubertov, V. V. Mironov, and N. N. Volkov, "Hybrid rocket engines: The benefits and prospects," Aerosp. Sci. Technol. **11**, 55–60 (2007).
[67]Y. Liu, P. Liu, Z. Wang, W. Ao, and Y. Guan, "Large eddy simulation of combustion instability in a subcritical hydrogen peroxide/kerosene liquid rocket engine: Intermittency route to period-2 thermoacoustic instability," Phys. Fluids **35**, 065145 (2023).
[68]Y. Liu, P. Liu, Z. Wang, W. Ao, and Y. Guan, "Numerical investigation of combustion instability in a single-element liquid rocket engine: Intermittency routes before and after thermoacoustic instability," Aerosp. Sci. Technol. **143**, 108691 (2023).
[69]Y. Guan, L. K. Li, H. Jegal, and K. T. Kim, "Effect of flame response asymmetries on the modal patterns and collective states of a can-annular lean-premixed combustion system," Proc. Combust. Inst. **39**, 4731–4739 (2023).
[70]Y. Guan, L. K. Li, B. Ahn, and K. T. Kim, "Chaos, synchronization, and desynchronization in a liquid-fueled diffusion-flame combustor with an intrinsic hydrodynamic mode," Chaos **29**, 053124 (2019).
[71]Y. Guan, K. Moon, K. T. Kim, and L. K. Li, "Synchronization and chimeras in a network of four ring-coupled thermoacoustic oscillators," J. Fluid Mech. **938**, A5 (2022).
[72]K. Moon, Y. Guan, L. K. Li, and K. T. Kim, "Mutual synchronization of two flame-driven thermoacoustic oscillators: Dissipative and time-delayed coupling effects," Chaos **30**, 023110 (2020).
[73]Y. Guan, Y. Choi, P. Liu, and K. T. Kim, "Mutual synchronization and flame dynamics in an axially fuel-staged lean-premixed combustion system," Proc. Combust. Inst. **40**, 105197 (2024).
[74]M. Ihme, W. T. Chung, and A. A. Mishra, "Combustion machine learning: Principles, progress and prospects," Prog. Energy Combust. Sci. **91**, 101010 (2022).
[75]M. Ihme and W. T. Chung, "Artificial intelligence as a catalyst for combustion science and engineering," Proc. Combust. Inst. **40**, 105730 (2024).